Journal of Molecular Liquids 322 (2021) 114900

Contents lists available at ScienceDirect

Journal of Molecular Liquids

journal homepage: www.elsevier.com/locate/molliq

Investigation on the impact of solvent on the photochemical properties of the photoactive anticancer drug Vemurafenib: A computational study

Abdulilah Dawoud Bani-Yaseen

Department of Chemistry & Earth Sciences, Faculty of Arts & Science, Qatar University, P.O. Box: 2713, Doha, Qatar

ARTICLE INFO

Article history:
Received 5 June 2020
Received in revised form 29 October 2020
Accepted 26 November 2020
Available online 28 November 2020

Keywords:
Vemurafenib
Phototoxicity
Microenvironment
Solvent effects
DFT/TD-DFT

ABSTRACT

Rationalizing the photochemical behavior of a photosensitive drug in terms of molecular properties is necessary toward understanding related potential phototoxicity. Here, we report on the effect of the molecular microenvironment on the physicochemical and photochemical properties of a first-line anticancer drug Vemurafenib. Time-dependent density functional (TD-DFT) calculations were performed to simulate the absorption spectra of Vemurafenib in implicit solvents of various polarity and hydrogen bonding capabilities. The obtained results revealed polarity-dependent spectral characteristics indicative of the influence of the microenvironment on the structural properties of the drug. In particular, a notable enhancement in the oscillation strength of the main electronic transition, namely HOMO→LUMO, was observed in polar solvents. These effects can be attributed to the enhanced charge delocalization across the molecule comprising the lone-pairs of the heteroatoms. Moreover, the obtained DFT results suggest that such electronic transition can exhibit a major influence on the photochemical properties of the drug. Furthermore, the effect of intermolecular hydrogen bonding between Vemurafenib and its microenvironment was explicitly investigated employing the same level of TD-DFT calculations. Obtained results demonstrated a substantial effect for such interactions on the spectral properties of the drug. In addition, the NBO analysis revealed physicochemical properties for the explicit hydrogen-bonded complexes of Vemurafenib with dimethylformamide molecules that are well in line with the TD-DFT results. These NBO results revealed substantial changes in the structural properties of the drug indicative of the influence of the intermolecular hydrogen bonding on its photochemical properties; this includes a notable change in the charge density of selected atoms as well as enhanced electronic transitions. The results reported herein provide insights concerning understanding the photochemical behavior of Vemurafenib in biologically mimicked microenvironments at the molecular level, which can be utilized in future efforts toward reducing induced phototoxicity.

1. Introduction

Photosensitivity of pharmaceuticals and associated potential phototoxicity are amongst the main concerns that can potentially lead to severe and undesired side effects [1–5]. The triggering process for phototoxicity is a photosensitizing stride that a photosensitive substance exhibits within a biological microenvironment under the influence of irradiating light. Photosensitization is a main interest with many beneficial applications for a broad spectrum of societies including the biomedical, pharmaceutical, and environmental societies [6–10]. With its remarkable applications, especially within the landscape of clinical and biomedical societies, photosensitization still can lead to undesired consequences that need to be addressed thoroughly [11–14]. A major concern in this regard is the side effects including the phototoxicity associated with the use of a wide spectrum of pharmaceuticals that can notably impact their therapeutic use [15–19]. As such, reducing such potential side effects is amongst the foremost interests of biomedical practitioners.

On the other hand, investigating the molecular properties of photosensitive pharmaceuticals is essential toward a better understanding of their pharmacokinetic performance and consequently reducing associated side effects. It is noteworthy mentioning that understanding the foundation of the drug's activities is crucial toward manipulating the origin of its potential side effects. In fact, a substance may undergo through unpredictable pathways upon being electronically excited, which in turn might be directing some pharmaceuticals into dangerous consequences. Fundamentally, a molecule at its excited state is expected to exhibit different physicochemical properties, such as the dipole moment, in comparison to the ground state as a result of the difference in the electronic distributions. Upon radiation-induced excitation, electrons in the ground state are promoted to an excited state resulting in new electronic distribution of enhanced charge separation. Such an enhanced charge separation can lead to increased dipole moment, which

E-mail address: abdulilah.baniyaseen@qu.edu.qa.

https://doi.org/10.1016/j.molliq.2020.114900
0167-7322/

in turn can induce a notable intermolecular interaction in polar molecular environment. Such difference in electronic distribution can induce different chemical reactivity that importantly needs to be elucidated under different microenvironments for a wide range of materials including pharmaceuticals [20–30].

In recent decades great interest has grown concerning the development and investigations of the drugs' activities and physicochemical properties at the molecular level [12,18,31–39]. More attention has been pointed to the photo mutagenic and photoallergic side effects induced by sunlight. For example, most of the reported findings concerning the phototoxicity of a first-line anticancer drug Vemurafenib (VFB) were constructed based on in vivo and in vitro investigations without taking into consideration the effects of the microenvironment at the molecular level. It is noteworthy mentioning that the phototoxicity of VFB may be attributed to some types of synergic effects under the presence of some species within the microenvironments of the drug, which in turn must be explored for reaching insightful information. Thus, it is very essential to elucidate the physicochemical behavior of such sensitive drugs at the molecular level under the effect of various architectures of microenvironments. To this end, elucidating potential intra−/inter-molecular interactions can be explicitly insightful toward promote our understanding of such kinds of microenviromental effects. In particular, various microenviromental factors can influence such kinds of intra−/inter-molecular interactions, such as the temperature and pH of the solution as well as the solvent parameters; the later factor incudes refractive index (n), dielectric constant (ε), polarity/polarizability, hydrophobicity/hydrophilicity, and hydrogen bonding capabilities [40,41]. Interestingly, constructing a framework regarding the interaction between a photosensitive pharmaceutical with its local microenvironment can reveal the major factors that influence the photosensitizing behavior, which in turn can be beneficial in developing methodologies and protocols that can enhance their clinical efficiency.

In the study reported herein, we provide computational insights concerning the effect of the nature of the molecular microenvironment on the physicochemical properties of the first-line anticancer drug Vemurafenib. The chemical structure of VFB is shown in Fig. 1. The solvent effects on the physicochemical properties of VFB are computationally examined employing various aspects of the density functional theory (DFT) approach. Time-dependent DFT approach (TD-DFT) was employed to simulate the absorption in solvents of various polarity index. The DFT and TD-DFT results were employed to rationalize and interpret the potential phototoxicity of VFB with the correspondence of its molecular properties.

2. Computational methods

All calculations were performed with *Gaussian 09* version D.01 [42]. Geometry optimization was performed employing the DFT method with the wB97XD functional 6–31 + G(d) basis set unless otherwise noted. The X-ray structural information of VFB obtained from the Cambridge Crystallographic Data Centre (CCDC) was utilized to construct the input structure for geometry optimization. The same input was utilized for all examined solvents, namely 1,4-dioxane, cyclohexane, DMF, DMSO, acetonitrile, isopropanol, methanol, water, as well as in the gas phase. The implicit solvent effect was incorporated employing the integral equation formalism polarizable continuum model (IEFPCM) [43]. The DFT/wB97XD(6-31G+(d))/IEFPCM optimized geometry in the solvent of interest is utilized as an input for simulating the absorption spectra of VFB in the corresponding solvent employing the TD-DFT method. For the TD-DFT method, three functional were tested and evaluated with the same basis set 6–31 + G(d), namely B3LYP, CAM-B3LYP, and wB97XD functionals. Natural bond orbital analysis (NBO) was employed as implemented in *Gaussian 09*. The multilinear regression analysis (MLRA) was performed using the Microsoft-Excel software.

3. Results and discussion

3.1. Geometry optimization

Although optimizing the geometry of the molecules under study does not provide conclusive insights concerning the molecule's reactivity, yet it is essential for performing other computational experiments including the simulation of the UV–Vis absorption spectra in the medium of interest. Fig. 2 displays the DFT/wB97XD(6-31G+(d))/IEFPCM (methanol) optimized geometry of VFB. The DFT functional of wB97XD has been particularly utilized to account for the non-covalent interactions including dispersion contributions [44–46]. As displayed in Fig. 2, the optimized geometry is in perfect match with the experimental structure concerning the major geometrical properties. Nevertheless, just a minor parameter was observed concerning the dihedral angle (C1-C2-C3-C4) that corresponds to twisted angle (see Fig. 2: ascribed as ∠α) between the 4-chlorophenyl and pyridine rings, where a value of 139° and 154° were obtained for the calculated geometry and experimental counterpart, respectively. However, in order to verify the source of difference in such dihedral angle, we examined another DFT functional and basis sets, namely DFT/M06-2×/6–311++G(d,p). In similar applicability to DFT/wB97XD, DFT/M06-2× has been demonstrated to exhibit excellent performance concerning the intra−/intermolecular interactions and dispersion contributions to the optimized geometry of molecules of interest [45,47]. Obtained results revealed no difference between DFT/wB97XD and DFT/M06-2× with basis set 6–311++G(d,p). As such, it can be suggested that such difference can be attributed to thte fact that the benchmarked geometry of VFB correspond to the geometry of the molecule in the solid state, whereas the DFT optimized geometry corresponds to the geometry of the molecule in the implicit solution.

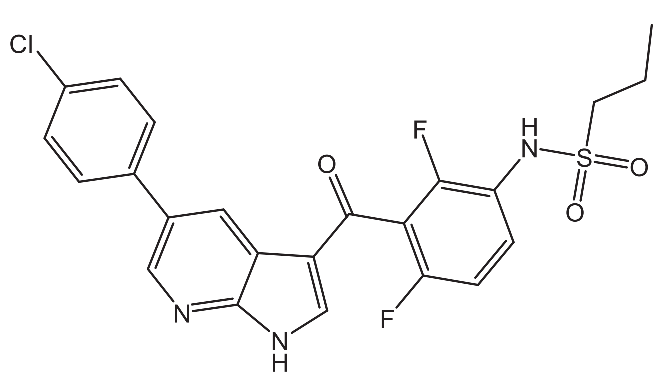

Fig. 1. Chemical structure of Vemurafenib.

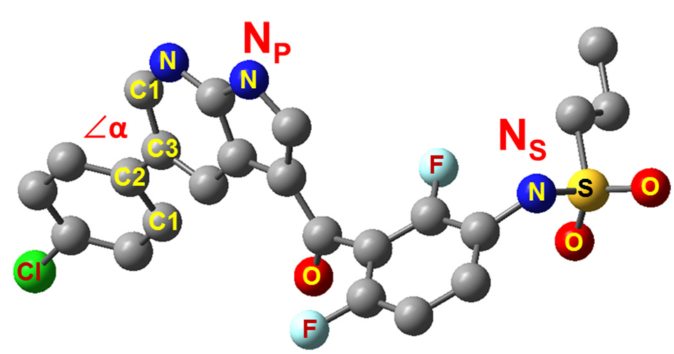

Fig. 2. DFT/wB97XD (6-31G+(d))/IEFPCM (methanol) optimized molecular geometry of VFB. Hydrogen atoms are omitted for clarity.

It is noteworthy to mention that it has been previously communicated that the VFB's moieties that are responsible for the photosensitivity of the drug are the secondary amines as illustrated in Fig. 2; these amine-groups are labeled as N-pyrrole (N_P) and N-sulfonamide (N_S) in Fig. 2 [37]. Importantly, the DFT calculations revealed structural parameters for these two moieties that are in excellent agreement with the experimental counterparts.

3.2. Simulated UV–Vis absorption spectra

In principle, it is noteworthy to mention that a photosafety assessment is generally performed within a spectral range that is relevant to the main spectral range of the sunlight that reaches the earth, namely 290–700 nm. As such, we focused herein on the spectral properties of VFB that is relevant to that specific spectral range. In particular, we investigated herein the solvent effects on the physicochemical properties of VFB concerning the potential effect of molecular microenvironment on the drug's photochemical properties. As a starting point for investigating the medium effect on the photochemical properties of VFB, the appropriateness of the employed TD-DFT method was examined via investigating the effect of the DFT functional used to simulate the absorption spectra of the drug. Fig. 3-left displays the simulated absorption spectra of VFB obtained employing the TD-DFT approach with three functionals namely B3LYP, CAM-B3LYP, and wB97XD using the same basis set of 6-31G+(d). Benchmarking of these simulated spectra was performed with respect to the reported experimental spectra [37,48]. According to the reported experimental absorption spectrum of VFB measured in methanol [48], the absorption spectrum exhibits two major bands with λ_{max1} and λ_{max2} of 306 and 253 nm, respectively, with intensity ratio (I_{306}:I_{253}) of 1:1.7. To this end, examining Fig. 3, it is worth noting that the absorption spectrum of VFB exhibits two absorption bands ascribed as λ_{max1} and λ_{max2} that are centered at wavelengths that depend on the DFT-functional applied. For example, using B3LYP functional, the calculation revealed λ_{max1} and λ_{max2} of 315 and 252 nm, respectively, whereas CAM-B3LYP and wB97XD functionals revealed λ_{max1} and λ_{max2} of 265 and 234 nm, respectively. These results are indicative of the more appropriateness of B3LYP functional for performing the TD-DFT calculations of the absorption spectra for VFB as it is in excellent agreement with the experimental counterparts. Henceforth, TD-DFT/ B3LYP (6-31G+(d)) method was employed for all other calculations unless otherwise noted.

3.3. Frontier molecular orbitals

In view of the absorption spectrum and potential photosensitive chromophores of VFB, it is necessary to elucidate the origin of the electronic transitions and the corresponding absorption band. As such, we performed a canonical molecular orbital (MO) analyses on the optimized geometry and the corresponding simulated spectra at the same level of DFT calculations. The TD-DFT results revealed that the absorption band of λ_{max1} corresponds solely to the excitation from the ground state (S0) to the first excited state (S1), i.e. S0 → S1 excitation with an oscillation strength ($\boldsymbol{f}_{\mathbf{o.s}}$) of 0.287, which is related to the transition from the highest occupied MO (HOMO) to the lowest unoccupied MO (LUMO), i.e. HOMO→LUMO transition. For the absorption band of λ_{max2}, the TD-DFT calculations revealed that S0 → S10 excitation has a predominant contribution with an $\boldsymbol{f}_{\mathbf{o.s}}$ of 0.442 and related mainly to the HOMO→LUMO+2 transition. Examining the shapes of frontier MOs (see Fig. 4), it is worth noting that the HOMO exhibits a delocalized shape that is extended over a conjugated π- system including the N_P moiety, whereas the LUMO extended over most parts of the molecule including the fluorine-substituted benzene ring and very close to the N_S moiety. As such, these results suggest that both absorption bands of λ_{max1} and λ_{max2} exhibit a $\pi \rightarrow \pi^*$ character. An Energy gap (HOMO-LUMO) of 4.46 eV was obtained for all polar solvents. In lights of these DFT results, it can be suggested that both photosensitive moieties N_S and N_P are potentially the origin of the photochemical behavior of VFB, which in turn is well in line with the experimental approach concerning the employment of photocaging of both moieties toward reducing the drug phototoxicity [37].

3.4. Implicit solvent effect and solvatochromic behavior of VFB

It is noteworthy to mention that a drug molecule can be surrounded by microenvironments of different polarities within a biological matrix. Thus, it is essential to explore the molecular properties of the drug under study in microenviromental conditions that resemble such biological matrices concerning polarity and potential intermolecular interactions. As such, we examined the implicit solvent effect on the

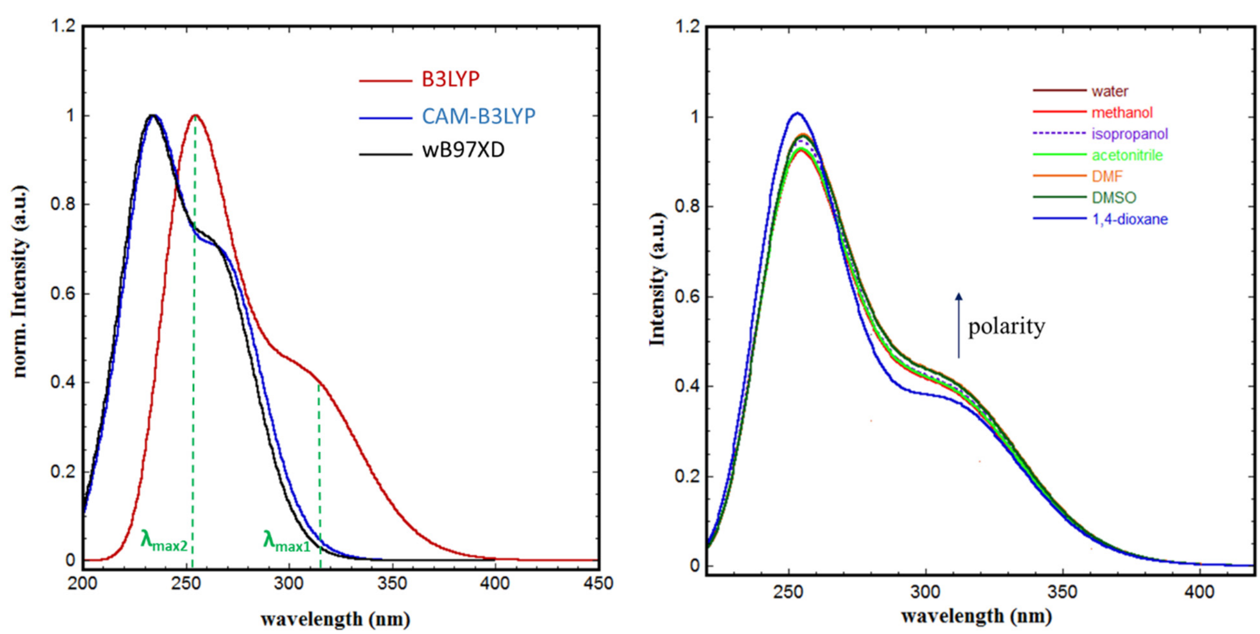

Fig. 3. DFT simulated UV–Vis absorption spectra of VFB; (left) in methanol using different functionals, (right) in different solvents. Same basis set (6–31 + G(d)) and IEFPCM model.

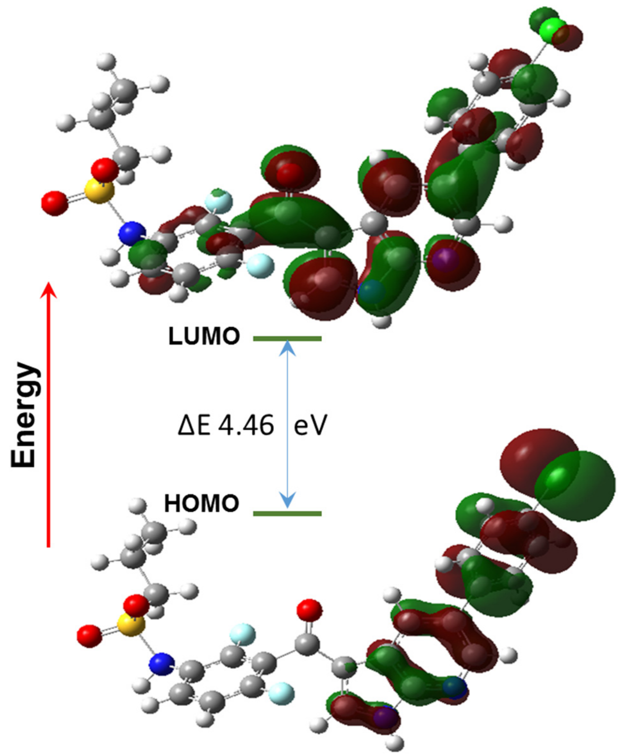

Fig. 4. Isosurfaces of the (canonical) frontier MOs (HOMO-LUMO) of VFB.

absorption spectra of VFB employing solvents of different polarity and hydrogen-bonding capabilities as illustrated in Fig. 3-right. As can be noted, a minor effect on the position of λ_{max1} was observed, where a bathochromic shift of only 1 nm is calculated in polar solvents compared to the nonpolar solvent 1,4-dioxane. However, it is worth noting that λ_{max1} exhibits a notable hyperchromic shift with increasing solvent polarity as indicated by the arrow in Fig. 3-right. The obtained DFT results suggest that such hyperchromic shift is indicative of increased $\mathbf{f_{o.s}}$ of the electronic transition in polar solvents that corresponds to the absorption band of λ_{max1}. For example a value of 0.268 and 0.300 was calculated for $\mathbf{f_{o.s}}$ in 1,4-dioxane and DMF, respectively. Such a change in the $\mathbf{f_{o.s}}$ might be attributed to the solvent-induced changes that the drug undergoes in its electronic states. The DFT results of $\mathbf{f_{o.s}}$ in all solvent studied herein as well as solvents' parameters are compiled in Table 1.

Furthermore, such changes in the spectral properties of VFB is indicative of the interaction between the drug with its microenvironment that might potentially induce changes on particular moieties or functional groups across the drug molecule. Hence, it is essential to rationalize such changes with respect to various parameters of the studied solvent. The first attempt was to correlate the $\mathbf{f_{o.s}}$ of λ_{max1} with the solvent orientation polarizability (Δf). Fig. 5-Left displays the obtained correlation for the polar protic and aprotic solvents. As can be noted, a good correlation with a regression coefficient (R) of 0.931 was achieved. On the other hand, it is worth noting that 1,4-dioxane was not considered in this correlation, where including this nonpolar solvent in the correlation relationship revealed a low value for R indicative of a poor correlation. On the other hand, in principle, Δf analysis does not reveal information concerning the hydrogen bonding effect of the solvent. As such, we performed further investigations herein by employing the Kamlet-Taft solvatochromic approach [49]. In this approach, the solvent effect is evaluated concerning the polarity of the solvent and its hydrogen bonding capabilities. The general form of this approach concerning $\mathbf{f_{o.s}}$ under solvent effect is given in Eq. (1):

$$\mathbf{f_{o.s}} = \mathbf{f_{o.s,g}} + a\alpha + b\beta + c\pi^* \quad (1)$$

where $\mathbf{f_{o.s,g}}$ is the oscillation strength in the gas phase; α and β are the hydrogen bond donor and acceptor, respectively; π^* is an index of solvents dipolarity/polarizability which reflects the capability of the solvent for stabilizing the dissolved dipole or charge; a, b and c are independent coefficients, where their magnitudes and signs indicate the effect of the corresponding solvent-solute interactions on the $\mathbf{f_{o.s}}$. We performed herein the multilinear regression analysis (MLRA) employing Eq. (1) for two sets of solvents, namely all solvents ($n = 7$) and polar solvents ($n = 6$), where 1,4-dioxane are omitted in the latter set. Obtained results of the MLRA are given in Eqs. (2) and (3).

$$\mathbf{f_{o.s}} = 0.2424 + 0.0014\boldsymbol{\alpha} + 0.0336\boldsymbol{\beta} + 0.0368\boldsymbol{\pi^*}\ R = 0.900, n = 7 \quad (2)$$

$$\mathbf{f_{o.s}} = 0.2718 – 0.0054\boldsymbol{\alpha} + 0.0178\boldsymbol{\beta} + 0.0174\boldsymbol{\pi^*}\ R = 0.989, n = 6 \quad (3)$$

One can notice that an excellent correlation of R = 0.989 was obtained for the polar set, whereas a relatively acceptable correlation of R = 0.900 was obtained with the consideration of the nonpolar solvent in the MLRA. The applicability of Eq. (3) to estimate implicitly the $\mathbf{f_{o.s(DFT)}}$ was evaluated via recalculating the $\mathbf{f_{o.s(MLRA)}}$. Obtained results are displayed in Fig. 5-Right. An excellent correlation with $R = 0.990$ was observed indicative of a considerable applicability of the MLRA. These MLRA results suggest that both factors of the solvents, namely polarity and hydrogen bonding capability, can affect the $\mathbf{f_{o.s}}$ of λ_{max1} of VFB and accordingly indicative of induced structural changes, which in turn might influence the drug's photochemical behavior.

3.5. Explicit solvent effect

The DFT results of the implicit solvent effect still necessitate performing an explicit solvent effect to account for possible intermolecular hydrogen bonding between VFB and its microenvironment. In light of the implicit solvent effect and functional groups of VFB that have potential photosensitivity, we examined herein the interaction of VFB with DMF molecules implicitly and explicitly. The DMF was selected as proof of principle in view of the DFT results obtained with implicit solvent effect as illustrated in Fig. 5, where implicit DMF microenvironment exhibited the most notable effect on the simulated absorption spectrum of VFB. For the explicit interaction of VFB with DMF, three configurations were considered. In the configurations A and B, 1:1 interactions is considered between VFB and one DMF molecule, where A and B correspond to hydrogen-bonding interaction with the N_P and N_S moieties of VFB, respectively. The third configuration is referred to as AB and it corresponds to 1:2 interaction between VFB and two DMF molecules, which is a combination of A and B. For these complexes, the N_S and N_P is the hydrogen bond donor (N—H), whereas the oxygen atom of the DMF molecule is the acceptor counterpart. The geometries of the hydrogen-bonded complexes were optimized at the same level of DFT

Table 1
solvent parameters and oscillation strength ($\mathbf{f_{o.s}}$) of λ_{max1} of VFB.

Solvent	ε	n	$\Delta f(\varepsilon,n)$[a]	π^*	α	β	$\mathbf{f_{o.s}}$
polar protic							
water	78.4	1.333	0.320	1.09	1.17	0.18	0.288
methanol	32.7	1.329	0.310	0.60	0.93	0.62	0.287
isopropanol	19.9	1.378	0.276	0.48	0.76	0.95	0.294
polar aprotic							
acetonitrile	36.6	1.344	0.305	0.75	0.19	0.31	0.289
DMSO	46.5	1.477	0.264	1.00	0	0.76	0.302
DMF	36.7	1.431	0.276	0.87	0	0.69	0.300
nonpolar							
1,4-Dioxane	2.2	1.422	0.022	0.55	0	0.37	0.268

[a] Orientation polarizability: $\Delta f = \frac{\varepsilon-1}{2\varepsilon+1} - \frac{n^2-1}{2n^2+1}$.

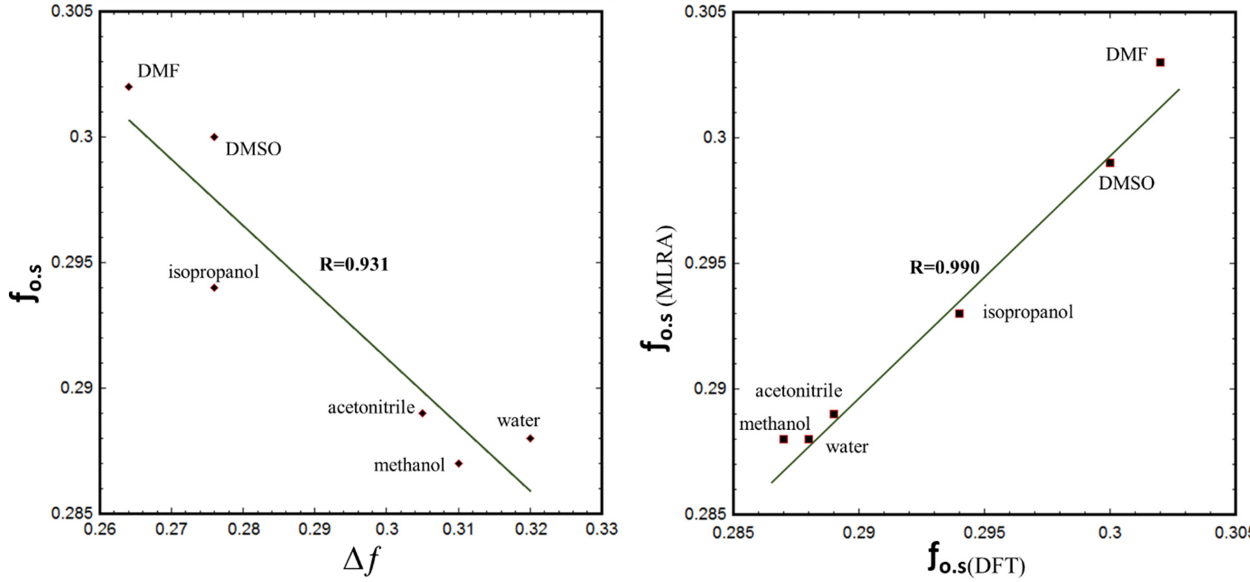

Fig. 5. Left: variation in the $\boldsymbol{f}_{\mathbf{o.s}}$ of λ_{max1} with the solvent orientation polarizability (Δf) (D; Right: Comparison between the DFT calculated and MLRA calculated $\boldsymbol{f}_{\mathbf{o.s}}$ of λ_{max1}.

calculations with implicit DMF microenvironment. The optimized geometries of all complexes with three configurations are displayed in Fig. 6. As can be noted in Fig. 6, a short hydrogen bond length ($d_{O\ldots H}$) was calculated for all complexes. For example, the DFT calculations revealed a $d_{O\ldots H}$ of 1.76 and 1.85 Å for the N_P-H → O_{DMF} and N_S-H → O_{DMF} for complexes A and B, respectively. Complex AB exhibited alike hydrogen-bonding behavior, where the calculations revealed a $d_{O\ldots H}$ of 1.76 and 1.78 Å for the two moieties of N_P-H → O_{DMF} and N_S-H → O_{DMF}, respectively. Additionally, we attempted to form the complex C, where VFB binds to DMF through bonding with Cl, using the same DFT method employed for other complexes. The obtained results revealed long distances for Cl…H(DMF) and Cl…O(DMF), where values of 3.972 and 3.123 Å were obtained, respectively. However, compared with other complexes, these distances are notably too long to be considered as significant stabilizing factors. As such, no further attempts were conducted for other clusters of C. It can be suggested that these results obtained from the attempts mentioned above are well in line with the molecular properties of DMF, where DMF is considered as a strong HB acceptor. These DFT results concerning the explicit solvent effect suggest a strong hydrogen bonding interaction between VFB and its microenvironment, which in turn was not feasible to be explored implicitly.

Importantly, although the geometry optimization process can reveal the structural properties of the VFB:DMF complexes, there is still a necessity for quantifying such interactions as well as examining and rationalizing other potential effects toward enhancing our understanding of the phototoxicity of the VFB drug. As such, we performed the NBO analysis at the same level of DFT calculations. Such calculations can reveal the energy of stabilization concerning the hydrogen bonding interaction for the VFB:DMF complexes as well as the NBO charges of all atoms involved in such interactions. The second-order perturbation energy (E(2)) obtained from the NBO analyses is employed herein as a measure of the relative strength of the hydrogen bonding. In this approach, the N_S-H → O_{DMF} hydrogen bond is presented as an electronic transition from the lone-pair of the oxygen (lp(O)) atom to the unoccupied orbital of the N—H bond (σ*). Such electronic transition is ascribed as lp(O) → σ*(N—H). As illustrated in Fig. 6, the superpositions of the NBOs involved in the hydrogen-bonding-based electronic transitions demonstrate the existence of such interaction. The overlapping regions between these NBOs demonstrate such interaction. The NBO analyses revealed an E(2) values of 23.6 and 43.3 kcal/mol for the lp(O) → σ*(N—H) of complexes A and B, respectively, indicative of strong hydrogen-bonding interaction between VFB and the DMF molecules. Likewise, complex AB exhibited alike behavior, where E(2) values of 21.0 and 19.8 kcal/mol were calculated for lp(O) → σ*(N_P-H) and lp(O) → σ*(N_S—H), respectively.

Furthermore, it is worth noting that lp(O) → σ*(N_P—H) was not affected by the coexistence of lp(O) → σ*(N_S-H), whereas the strength of lp(O) → σ*(N_S-H) was reduced by approximately 50%. It can be suggested herein that such coexistence of hydrogen bondings can induce structural changes in the VFB molecule that might affect its physicochemical properties. As such, we further analyzed the effect of such explicit hydrogen bonding on other structural properties. In particular, we performed an NBO charge (Q_{NBO}) analysis as well as geometrical analyses for selected bonds. Obtained results revealed QNBO values of −0.541 and −0.913 for N_P and N_S, respectively for VFB in implicit DMF solvent. The Q_{NBO} values calculated for all complexes concerning the nitrogen atoms of the N—H bond of both N_P and N_S moieties were compared with the values obtained for VFB in implicit solvent microenvironment. Obtained results revealed an increase in the negative Q_{NBO} by 0.015 for both moieties indicative of increasing the charge density on the nitrogen atom, which is well in line with the E(2) values obtained for the lp(O) → σ*(N—H) electronic transitions. In addition, the length of N—H has dramatically increased by 0.017 and 0.024 Å for the N_P and N_S moieties, respectively, because of such hydrogen-bonding interactions.

In light of the frontier MOs and NBO analyses, it can be suggested that the lp of both nitrogen atoms of N_P and N_S moieties are involved in the conjugation systems, with more contribution from the N_S moiety. Hence, it can be suggested that hydrogen bonding might influence such conjugation and consequently affect the HOMO→LUMO electronic transitions. As such, we performed TD-DFT calculations for all complexes and compared it with the results obtained for VFB in implicit DMF solvent. Fig. 7 displays the DFT simulated spectra for all studied molecules.

It is noteworthy mentioning that although the absorption band of λ_{max1} appears as a shoulder in the spectrum, yet the TD-DFT calculations can specifically indicate the exact wavelength of the corresponding electronic transition of the absorption band or shoulder of interest. As shown in Fig. 7, a notable change was observed in the absorption spectrum of VFB in implicit DMF solvent upon complexation explicitly with DMF molecules. On the other hand, it is important to mention that the DFT calculations revealed similar frontier MOs for all complexes indicative of alike type of electronic transition for the absorption band of

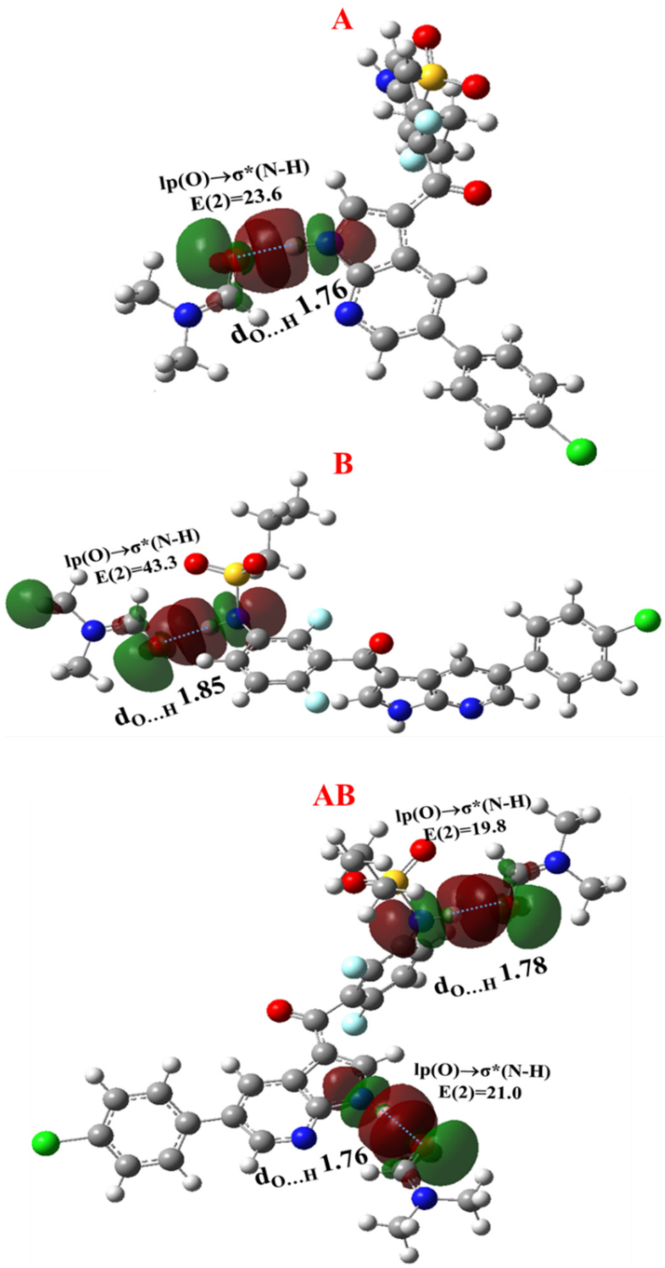

Fig. 6. Optimized geometries and **s**uperpositions of selected NBOs of the VFP:DMF hydrogen-bonded complexes; the given numbers indicate the length of the hydrogen bond ($d_{O...H}$, Å) and the second-order perturbation energy E(2) in kcal/mol.

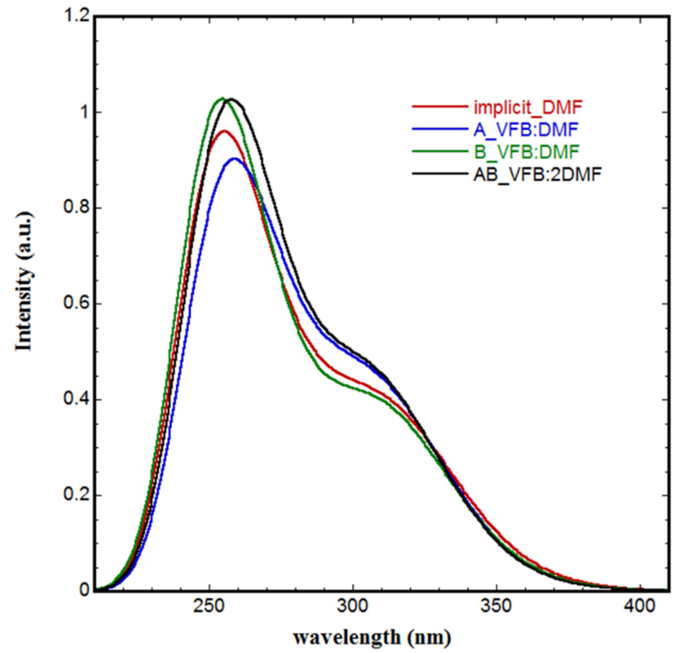

Fig. 7. DFT simulated absorption spectra of VFB:DMF complexes in implicit DFM solvent.

λ_{max1}; i.e. HOMO→LUMO transitions of the $\pi \rightarrow \pi^*$ character. Interestingly, the TD-DFT calculations revealed a hypsochromic shift of 3.3, 2.4, and 4.6 nm in λ_{max1}, for complexes A, B, and AB, respectively. These results suggest that the hypsochromic shift is indicative of stabilized ground state induced by hydrogen bonding. Such stabilization can be attributed to the enhanced charge delocalization across the π-conjugation system of the VFB molecule. It can be noted that the calculations indicate a hyperchromic shift in the spectrum, where the results revealed an increase of 0.033, 0.015, and 0.049 in the $\boldsymbol{f_{o.s}}$ of λ_{max1} for complexes A, B, and AB, respectively. This type of hyperchromic shift might be attributed to the upsurge in the charge density on the nitrogen atom and consequently enhanced the probability of the HOMO→LUMO electronic transition. These TD-DFT suggest substantial changes in the structural properties of the VFB molecules induced by hydrogen bonding complexations with its local microenvironment, which are well in line with the results obtained from the DFT geometry optimization. Hence, it can be suggested herein that the phototoxicity of VFB is associated with its microenvironment-dependent physicochemical properties.

4. Concluding remarks

The present work provides DFT computational insights on the solvent effects on the physicochemical and photochemical properties of an important anticancer drug VFB. The DFT and TD-DFT results demonstrated a substantial microenvironment effect on the structural properties of the drug that may have a significant impact on its photochemical behavior and associated phototoxicity. In particular, VFB exhibited an implicit solvent-dependent spectral behavior. Hence, the probability of a specific electronic transition has notably exhibited a hyperchromic shift with increasing solvent polarity. In light of the implicit solvent effect, the explicit influence of the microenvironment was demonstrated via investigating the complexation of VFB with DMF molecules employing the TD-DFT and NBO approaches. The obtained results suggest a strong hydrogen-bonded complex that can potentially influence selected structural properties of VFB including the main electronic transition in the absorption spectrum of the drug. On the other hand, it is important to mention that such electronic transitions have been previously communicated to be significant in inducing an unstable photochemical behavior for the drug. As such, the results reported herein can be utilized toward enhancing the photostability of VFB and consequently reducing its phototoxicity.

Declaration of Competing Interest

None.

Acknowledgments

This work was supported by the Qatar University [QUCD-CAS-2020-1]. Major aspects of the calculations were performed using the supercomputing facility at Texas A&M University at Qatar. Open Access funding provided by the Qatar National Library.

References

[1] S.M. O'Gorman, G.M. Murphy, Photosensitizing medications and photocarcinogenesis, Photodermatol. Photoimmunol. Photomed. 30 (2014) 8–14, https://doi.org/10.1111/phpp.12085.

[2] G. Cosa, Photodegradation and photosensitization in pharmaceutical products: assessing drug phototoxicity, Pure Appl. Chem. 76 (2004) 263–275, https://doi.org/10.1351/pac200476020263.

[3] S. Monti, S. Sortino, Photoprocesses of photosensitizing drugs within cyclodextrin cavities, Chem. Soc. Rev. 31 (2002) 287–300, https://doi.org/10.1039/b106751f.

[4] G. Halliday, S. Byrne, J. Lyons, D. Damian, Photocarcinogenesis nonmelanoma skin cancer, Handb. Photomed, Taylor & Francis 2013, pp. 69–80, https://doi.org/10.1201/b15582-10.

[5] K.A. Su, L.A. Habel, N.S. Achacoso, G.D. Friedman, M.M. Asgari, Photosensitizing antihypertensive drug use and risk of cutaneous squamous cell carcinoma, Br. J. Dermatol. 179 (2018) 1088–1094, https://doi.org/10.1111/bjd.16713.

[6] M. Ichihashi, M. Ueda, A. Budiyanto, T. Bito, M. Oka, M. Fukunaga, K. Tsuru, T. Horikawa, UV-induced skin damage, Toxicology. 189 (2003) 21–39, https://doi.org/10.1016/S0300-483X(03)00150-1.

[7] J. Cadet, T. Douki, Formation of UV-induced DNA damage contributing to skin cancer development, Photochem. Photobiol. Sci. 17 (2018) 1816–1841, https://doi.org/10.1039/C7PP00395A.

[8] D.L. Narayanan, R.N. Saladi, J.L. Fox, Review: ultraviolet radiation and skin cancer, Int. J. Dermatol. 49 (2010) 978–986, https://doi.org/10.1111/j.1365-4632.2010.04474.x.

[9] K. Rass, J. Reichrath, UV damage and DNA repair in malignant melanoma and nonmelanoma skin cancer, Sunlight, Vitam. D Ski. Cancer, Springer New York, New York, NY 2008, pp. 162–178, https://doi.org/10.1007/978-0-387-77574-6_13.

[10] A. Sample, Y.-Y. He, Mechanisms and prevention of UV-induced melanoma, Photodermatol. Photoimmunol. Photomed. 34 (2018) 13–24, https://doi.org/10.1111/phpp.12329.

[11] A.F. Monteiro, M. Rato, C. Martins, Drug-induced photosensitivity: Photoallergic and phototoxic reactions, Clin. Dermatol. 34 (2016) 571–581, https://doi.org/10.1016/j.clindermatol.2016.05.006.

[12] F. Schmidt, J. Wenzel, N. Halland, S. Güssregen, L. Delafoy, A. Czich, Computational investigation of drug phototoxicity: photosafety assessment, photo-toxophore identification, and machine learning, Chem. Res. Toxicol. 32 (2019) 2338–2352, https://doi.org/10.1021/acs.chemrestox.9b00338.

[13] T.A. Duong, L. Valeyrie-Allanore, P. Wolkenstein, O. Chosidow, Severe cutaneous adverse reactions to drugs, Lancet. 390 (2017) 1996–2011, https://doi.org/10.1016/S0140-6736(16)30378-6.

[14] S. Peukert, J. Nunez, F. He, M. Dai, N. Yusuff, A. DiPesa, K. Miller-Moslin, R. Karki, B. Lagu, C. Harwell, Y. Zhang, D. Bauer, J.F. Kelleher, W. Egan, A method for estimating the risk of drug-induced phototoxicity and its application to smoothened inhibitors, Medchemcomm. 2 (2011) 973, https://doi.org/10.1039/c1md00144b.

[15] R. Kreutz, E.A.H. Algharably, A. Douros, Reviewing the effects of thiazide and thiazide-like diuretics as photosensitizing drugs on the risk of skin cancer, J. Hypertens. 37 (2019) 1950–1958, https://doi.org/10.1097/HJH.0000000000002136.

[16] W. Ben Kim, A.J. Shelley, K. Novice, J. Joo, H.W. Lim, S.J. Glassman, Drug-induced phototoxicity: a systematic review, J. Am. Acad. Dermatol. 79 (2018) 1069–1075, https://doi.org/10.1016/j.jaad.2018.06.061.

[17] A.M. Drucker, C.F. Rosen, Drug-induced photosensitivity, Drug Saf. 34 (2011) 821–837, https://doi.org/10.2165/11592780-000000000-00000.

[18] B. Henry, C. Foti, K. Alsante, Can light absorption and photostability data be used to assess the photosafety risks in patients for a new drug molecule? J. Photochem. Photobiol. B Biol. 96 (2009) 57–62, https://doi.org/10.1016/j.jphotobiol.2009.04.005.

[19] K. Kim, H. Park, K.-M. Lim, Phototoxicity: its mechanism and animal alternative test methods, Toxicol. Res. 31 (2015) 97–104, https://doi.org/10.5487/TR.2015.31.2.097.

[20] N.S. Gould, S. Li, H.J. Cho, H. Landfield, S. Caratzoulas, D. Vlachos, P. Bai, B. Xu, Understanding solvent effects on adsorption and protonation in porous catalysts, Nat. Commun. 11 (2020) 1060, https://doi.org/10.1038/s41467-020-14860-6.

[21] A. Marini, A. Muñoz-Losa, A. Biancardi, B. Mennucci, What is Solvatochromism? J. Phys. Chem. B 114 (2010) 17128–17135, https://doi.org/10.1021/jp1097487.

[22] P.F. Barbara, G.C. Walker, T.P. Smith, Vibrational modes and the dynamic solvent effect in electron and proton transfer, Science (80-.). 256 (1992) 975–981, https://doi.org/10.1126/science.256.5059.975.

[23] A.D. Bani-Yaseen, F. Hammad, B.S. Ghanem, E.G. Mohammad, On the photophysicochemical properties of selected fluoroquinolones: solvatochromic and fluorescence spectroscopy study, J. Fluoresc 23 (1) (2013) 93–101, https://doi.org/10.1007/s10895-012-1120-7.

[24] E. Buncel, S. Rajagopal, Solvatochromism and solvent polarity scales, Acc. Chem. Res. 23 (1990) 226–231, https://doi.org/10.1021/ar00175a004.

[25] M.M. Miotke, M. Józefowicz, Solvatochromism of antiinflammatory drug – naproxen sodium, J. Mol. Liq. 230 (2017) 129–136, https://doi.org/10.1016/j.molliq.2016.12.094.

[26] A.D. Bani-Yaseen, M. Al-Balawi, The solvatochromic, spectral, and geometrical properties of nifenazone: a DFT/TD-DFT and experimental study, Phys. Chem. Chem. Phys. 16 (2014) 15519–15526, https://doi.org/10.1039/C4CP01679C.

[27] T.J. Zuehlsdorff, P.D. Haynes, F. Hanke, M.C. Payne, N.D.M. Hine, Solvent effects on electronic excitations of an organic chromophore, J. Chem. Theory Comput. 12 (2016) 1853–1861, https://doi.org/10.1021/acs.jctc.5b01014.

[28] A.D. Bani-Yaseen, Solvatochromic and fluorescence behavior of sulfisoxazole, J. Fluoresc. 21 (2011) 1061–1067, https://doi.org/10.1007/s10895-010-0778-y.

[29] C. Reichardt, T. Welton, Solvents and Solvent Effects in Organic Chemistry, Fourth edition Reichardt - Wiley Online Library, 4th ed., Wiley-VCH, 2010 http://onlinelibrary.wiley.com/book/10.1002/9783527632220 (accessed March 8, 2016).

[30] C. Reichardt, Solvents and solvent effects: an introduction, Org. Process. Res. Dev. 11 (2007) 105–113, https://doi.org/10.1021/op0680082.

[31] C. Imberti, P. Zhang, H. Huang, P.J. Sadler, New designs for phototherapeutic transition metal complexes, Angew. Chem. Int. Ed. 59 (2020) 61–73, https://doi.org/10.1002/anie.201905171.

[32] Z. Li, A. David, B.A. Albani, J.-P. Pellois, C. Turro, K.R. Dunbar, Optimizing the electronic properties of photoactive anticancer oxypyridine-bridged dirhodium(II,II) complexes, J. Am. Chem. Soc. 136 (2014) 17058–17070, https://doi.org/10.1021/ja5078359.

[33] A.D. Bani-Yaseen, Computational molecular perspectives on the interaction of propranolol with β-cyclodextrin in solution: towards the drug-receptor mechanism of interaction, J. Mol. Liq. 227 (2017) 280–290, https://doi.org/10.1016/j.molliq.2016.12.023.

[34] S. Miyata, M. Hoshino, T. Isozaki, T. Yamada, H. Sugimura, Y.-Z. Xu, T. Suzuki, Acid dissociation equilibrium and singlet molecular oxygen quantum yield of acetylated 6,8-dithioguanosine in aqueous buffer solution, J. Phys. Chem. B 122 (2018) 2912–2921, https://doi.org/10.1021/acs.jpcb.8b00517.

[35] H. Imai, V. Kefalov, K. Sakurai, O. Chisaka, Y. Ueda, A. Onishi, T. Morizumi, Y. Fu, K. Ichikawa, K. Nakatani, Y. Honda, J. Chen, K.-W. Yau, Y. Shichida, Molecular properties of rhodopsin and rod function, J. Biol. Chem. 282 (2007) 6677–6684, https://doi.org/10.1074/jbc.M610086200.

[36] A.D. Bani-Yaseen, Synchronous spectrofluorimetric study of the supramolecular host–guest interaction of β-cyclodextrin with propranolol: a comparative study, Spectrochim. Acta Part A Mol. Biomol. Spectrosc. 148 (2015) 93–98, https://doi.org/10.1016/j.saa.2015.03.128.

[37] R. Horbert, B. Pinchuk, P. Davies, D. Alessi, C. Peifer, Photoactivatable prodrugs of antimelanoma agent vemurafenib, ACS Chem. Biol. 10 (2015) 2099–2107, https://doi.org/10.1021/acschembio.5b00174.

[38] T. Wei, S. Lu, J. Sun, Z. Xu, X. Yang, F. Wang, Y. Ma, Y.S. Shi, X. Chen, Sanger's reagent sensitized photocleavage of amide bond for constructing photocages and regulation of biological functions, J. Am. Chem. Soc. 142 (2020) 3806–3813, https://doi.org/10.1021/jacs.9b11357.

[39] A.D. Bani-Yaseen, Computational insights into the photocyclization of diclofenac in solution: effects of halogen and hydrogen bonding, Phys. Chem. Chem. Phys. 18 (2016) 21322–21330, https://doi.org/10.1039/c6cp03671f.

[40] M. Homocianu, A. Airinei, Intra−/inter-molecular interactions – identification and evaluation by optical spectral data in solution, J. Mol. Liq. 225 (2017) 869–876, https://doi.org/10.1016/j.molliq.2016.11.013.

[41] J. Catalán, Toward a generalized treatment of the solvent effect based on four empirical scales: dipolarity (SdP, a new scale), polarizability (SP), acidity (SA), and basicity (SB) of the medium, J. Phys. Chem. B 113 (2009) 5951–5960, https://doi.org/10.1021/jp8095727.

[42] G.E. Frisch, M. J.; Trucks, G. W.; Schlegel, H. B.; Scuseria, V. M. Robb, M. A.; Cheeseman, J. R.; Scalmani, G.; Barone, H. B.; Petersson, G. A.; Nakatsuji, H.; Caricato, M.; Li, X.; Hratchian, M. P.; Izmaylov, A. F.; Bloino, J.; Zheng, G.; Sonnenberg, J. L.; Hada, M. N. Ehara, M.; Toyota, K.; Fukuda, R.; Hasegawa, J.; Ishida, J. T.; Honda, Y.; Kitao, O.; Nakai, H.; Vreven, T.; Montgomery, J. A., E.N.. Peralta, J. E.; Ogliaro, F.; Bearpark, M. J.; Heyd, J.; Brothers, J. Kudin, K. N.; Staroverov, V. N.; Kobayashi, R.; Normand, S.S.. Raghavachari, K.; Rendell, A. P.; Burant, J. C.; Iyengar, J.E. Tomasi, J.; Cossi, M.; Rega, N.; Millam, N. J.; Klene, M.; Knox, R.. Cross, J. B.; Bakken, V.; Adamo, C.; Jaramillo, J.; Gomperts, C. Stratmann, R. E.; Yazyev, O.; Austin, A. J.; Cammi, R.; Pomelli, V.G.. Ochterski, J. W.; Martin, R. L.; Morokuma, K.; Zakrzewski, A. Voth, G. A.; Salvador, P.; Dannenberg, J. J.; Dapprich, S.; Daniels, D.J. D.; Farkas, O.; Foresman, J. B.; Ortiz, J. V.; Cioslowski, J.; Fox, Gaussian 09, Gaussian, Inc. Wallingford, CT,. (n.d.).

[43] J. Tomasi, B. Mennucci, E. Cancès, The IEF version of the PCM solvation method: an overview of a new method addressed to study molecular solutes at the QM ab initio level, J. Mol. Struct. THEOCHEM 464 (1999) 211–226, https://doi.org/10.1016/S0166-1280(98)00553-3.

[44] N. Mardirossian, M. Head-Gordon, Thirty years of density functional theory in computational chemistry: an overview and extensive assessment of 200 density functionals, Mol. Phys. 115 (2017) 2315–2372, https://doi.org/10.1080/00268976.2017.1333644.

[45] Y. Zhao, D.G. Truhlar, Density functionals with broad applicability in chemistry, Acc. Chem. Res. 41 (2008) 157–167, https://doi.org/10.1021/ar700111a.

[46] A.I. Lazar, F. Biedermann, K.R. Mustafina, K.I. Assaf, A. Hennig, W.M. Nau, Nanomolar binding of steroids to cucurbit[n]urils: selectivity and applications, J. Am. Chem. Soc. 138 (2016) 13022–13029, https://doi.org/10.1021/jacs.6b07655.

[47] D.V. Wagle, H. Zhao, C.A. Deakyne, G.A. Baker, Quantum chemical evaluation of deep eutectic solvents for the extractive desulfurization of fuel, ACS Sustain. Chem. Eng. 6 (2018) 7525–7531, https://doi.org/10.1021/acssuschemeng.8b00224.

[48] P. Morlière, F. Boscá, A.M.S. Silva, A. Teixeira, A. Galmiche, J.-C. Mazière, V. Nourry, J. Ferreira, R. Santus, P. Filipe, A molecular insight into the phototoxic reactions observed with vemurafenib, a first-line drug against metastatic melanoma, Photochem. Photobiol. Sci. 14 (2015) 2119–2127, https://doi.org/10.1039/C5PP00231A.

[49] M.J. Kamlet, J.L.M. Abboud, M.H. Abraham, R.W. Taft, Linear solvation energy relationships. 23. A comprehensive collection of the solvatochromic parameters, .pi.*, .alpha., and .beta., and some methods for simplifying the generalized solvatochromic equation, J. Organomet. Chem. 48 (1983) 2877–2887, https://doi.org/10.1021/jo00165a018.